*and Cheng-Maw Cheng and their collaborators published in ACS Nano **15**, 15085 (2021).*

TLS 21B1 Angle-resolved UPS

- ARPES
- Materials Science, Condensed-matter Physics

Reference

1. S. H. Su, P.-Y. Chuang, H.-Y. Chen, S.-C. Weng, W.-C. Chen, K.-D. Tsuei, C.-K. Lee, S.-H. Yu, M. M.-C. Chou, L.-W. Tu, H.-T. Jeng, C.-M. Tu, C.-W. Luo, C.-M. Cheng, T.-R. Chang, J.-C. A. Huang, ACS Nano **15**, 15085 (2021).

A Hallmark of Hund's Physics in the Multi-Orbital System

An abrupt deviation from Fermi liquid behavior has been directly observed in electron self-energy results as the kink feature at a low-energy scale. The results of the evolution of the characteristic temperature scale via a kink features, which is a hallmark of Hund's physics in a multi-orbital system.

Since Mott's initial proposal that an insulating ground state can appear due to the electron–electron correlation, the metal-insulator transition (MIT) has been at the core of condensed-matter physics. The Coulomb interaction U is the most important parameter; thus finding how the spectral function and energy scale evolve as a function of U has been a fundamental issue in MIT studies. The Brinkman-Rice picture and dynamical mean-field theory (DMFT) for the half-filled one-band Hubbard model show that the overall quasi-particle (QP) peak and Kondo temperature T_K gradually become renormalized as U increases. At the MIT, the QP mass diverges with vanishing T_K. Most realistic materials are, however, multi-orbital systems in which not only U but also Hund's coupling J_H is a critical parameter for the ground state. During the past decade, there has been a remarkable progress in the theoretical description of Hund's physics in correlated electron systems. It was found that J_H can enhance the effective correlation strength of multi-orbital systems by weakening the Kondo screening channel. The most drastic effect occurs in non-singly-occupied and non-half-filled cases such as iron pnictides, chalcogenides and ruthenates. Although these materials are metallic and are located far from the Mott insulating state, their small coherence energy scale due to J_H induces incoherent transport properties. These new phases are classified as Hund's metal; their correlated electronic structures have been intensively studied through both experimental and theoretical approaches.

An important remaining question is how J_H affects the evolution of the spectral function and the energy scale of multiband systems. Considering these aspects, $NiS_{2-x}Se_x$, a half-filled system with degenerate Ni e_g orbitals, is probably the most suitable multi-orbital system for an investigation of the evolution in the presence of J_H. On varying the Se content, the correlation strength can be easily tuned in the existence of J_H. To address the role of J_H during the MIT, Changyoung Kim (Seoul National University, Korea), Cheng-Maw Cheng (NSRRC) and their teams reexamined the band structure of $NiS_{2-x}Se_x$ not only with angle-resolved photoemission spectra (ARPES) with finer doping steps and higher resolution but also *via* density-functional theory (DFT) plus DMFT with and without J_H. They utilized ARPES to achieve the high resolution needed to observe clearly the QP of $NiS_{2-x}Se_x$. Their results reveal clear QP dispersions as well as doping-dependent low-energy kink structures. The DFT+DMFT calculations also identify the kink structures, which explain the strongly suppressed temperature scale due to J_H. The evolution of a kink observed in their ARPES data provides direct spectroscopic evidence for the evolution of the energy scale in the presence of J_H.

The α hole pocket is the most representative QP band for the Mott transition in $NiS_{2-x}Se_x$. As the Fermi-surface volume of the α band is much larger than the others, the transport properties of $NiS_{2-x}Se_x$ should be dominated by the hole pocket. To study how the α band dispersion varies across the MIT, they performed ARPES experiments at **TLS 21B1** beamline of the NSRRC. ARPES spectra along the Γ-X line were recorded at 16 K for diverse Se doping shown in **Fig. 1**. A QP band, distinct from the incoherent band (**Fig. 1(g)**), is clearly observed in all metallic samples, whereas the QP was not clearly discernible as it was buried under an incoherent spectral weight in previous reports (grey filled curve in **Fig. 1(g)**). The appearance or disappearance of the QP follows the MIT behavior along the Se doping; the QP is seen for the metallic phase ($x \geq 0.43$) whereas it is absent in the insulating phase ($x = 0.3$) (see **Fig. 1(a)** for the phase diagram).

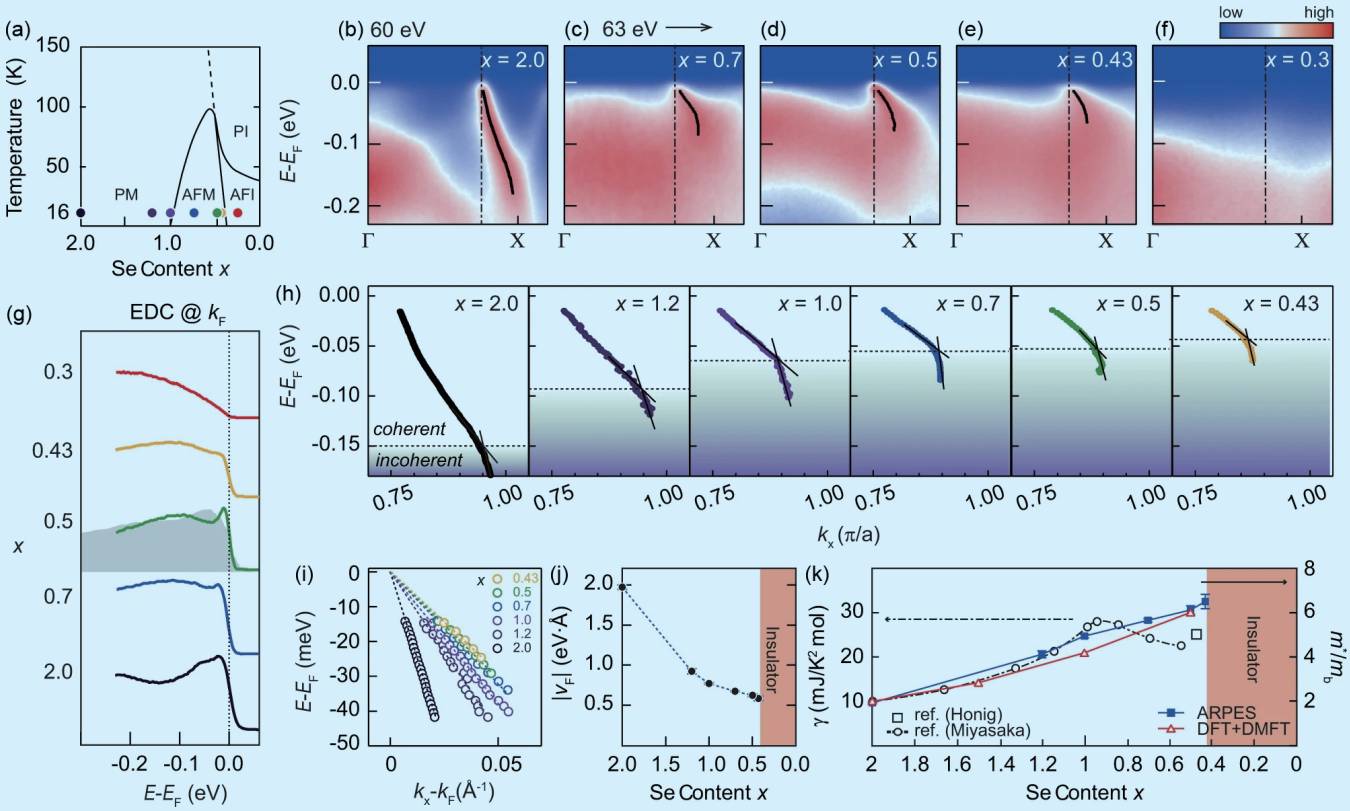

Fig. 1: Se content-dependent QP dispersion. (a) Phase diagram of $NiS_{2-x}Se_x$. (b–f) ARPES data along direction Γ-X. (g) Energy distribution curves (EDC) at the Fermi momentum (k_F) as represented by dashed-dotted lines in panels (b–f). (h) QP dispersions obtained on fitting momentum distribution curves. (i–k) Doping-dependent band dispersion, Fermi velocity v_F and effective mass m*, respectively. The linear coefficient of the specific heat γ is also plotted for comparison. [Reproduced from Ref. 1]

An important aspect of the data in **Fig. 1** is that a kink feature is observed in the dispersion for all metallic systems. Such a kink feature is normally interpreted to arise from electron-phonon coupling, but the energy scale of the kink, especially for $NiSe_2$, is too large to have a phonon origin. In addition, the kink moves toward the lower-energy side as the molar mass decreases (that is, as S content increases), which is opposite what is expected from the electron-phonon interaction. Magnons and plasmons can also be excluded as the origin of the kink. If the kink originates from electron-magnon interaction, the energy scale of the kink is expected to increase as the system approaches the Mott insulating phase (that is, as S content increases). In contrast, plasmons have a much larger energy scale (few eV or greater) than the kink energy in the data. Another notable aspect of the kink feature is that the kink becomes stronger as the system approaches the Mott insulating phase, alluding to its possible connection to the MIT. Previous theoretical studies predicted that a strongly renormalized coherent part is confined to a low-energy scale set by J_H. This effect explains why the kinks are generally found at the low-energy scale in a Hund's metal. This hallmark of J_H survives even in the vicinity of MIT at which U is dominant. Their ARPES data in **Fig. 2(h)** provide direct spectroscopic information on how the kink induced by J_H evolves as ratio U/W increases. The kink moves toward the lower-energy scale as the system approaches the Mott insulating phase.

In summary, the research team directly observed an evolution of the coherence energy scale *via* a kink feature. The ARPES data presented here show how the kink from J_H evolves as the correlation strength increases. From DFT+DMFT calculations, they have confirmed that this kink originates from J_H and is related to the crossing temperature scale. The suppression of Kondo screening by J_H implements the kink feature at the low-energy scale; the kink moves toward the lower-energy side as the correlation strength further increases with S doping. Their results clearly demonstrate that the evolution of a kink can be understood by the evolution of the characteristic energy scale. (Reported by Cheng-Maw Cheng)

This report features the work of Changyoung Kim, Cheng-Maw Cheng and their collaborators published in Nat. Commun. ***12****, 1208 (2021).*

TLS 21B1 Angle-resolved UPS

- High-resolution ARPES
- Materials Science, Condensed-matter Physics

Reference

1. B. G. Jang, G. Han, I. Park, D. Kim, Y. Y. Koh, Y. Kim, W. Kyung, H.-D. Kim, C.-M. Cheng, K.-D. Tsuei, K. D. Lee, N. Hur, J. H. Shim, C. Kim, G. Kotliar, Nat. Commun. **12**, 1208 (2021).

Miniaturize Floating-Gate Transistors to Approach a Physical Limit

On modulating the amount of electric-field-induced trapped electrons with an electrostatic gate potential, the demonstrated characteristics indicate that the engineering of an InSe interface has potential applications for nonvolatile memory.

Van-der-Waals-bonded layered materials enable the isolation and subsequent construction of heterostructures with designer interfaces and without constraint of lattice matching. Such interface engineering provides a knob that controls the electron behaviors of the artificial structures by controlling the interactions between layers through variations in the symmetry, stacking angles and chemical composition. These layered structures have been incorporated into a nonvolatile memory cell to mimic the conventional setup in which a floating gate generates a long-lasting internal electric field. In the applications of transistor-type nonvolatile memory cells, stacks of graphene and insulating oxide have been incorporated to scale the floating gate (polysilicon/SiO_2), in which a long-lasting internal electric field continuously modulates the carrier concentration in the channel. In these heterostructures, charges are confined in the floating gate because of a difference in the barrier height of interface energy between the layered materials and the insulating oxides. Upon continuous device scaling, however, progress is hampered by diffraction-limited photolithography and nonscalable tunneling oxide thicknesses that contribute to, for example, back tunneling. Innovations in cell architecture, decreased fabrication complexity and new device materials are thus in high demand.

Yi-Ying Lu (National Sun Yat-sen University), Chia-Hao Chen (NSRRC) and their teams proposed a new device concept that uses the van der Waals gating effect resulting from long-lived localized charges on the surface layer of InSe, which acts as an effective gate and which is separated by the van der Waals gap and generates a stable electron-storage effect in the underlying InSe channel. In contrast to a conventional flash memory cell in which charges are confined within potential wells formed by gate dielectric and semiconductor stacks, the charges in their structure are localized by trap sites generated by an indirect oxygen plasma treatment. Moreover, the channel current levels in InSe devices can be modulated on tuning the amounts of localized charge through the application of various back-gate voltages (V_G), enabling multilevel data storage.

To construct a back-gated field effect transistor (FET), two electrodes were deposited on both ends of InSe. The small bias current and bias voltage (I_{DS}–V_{DS}) measured at various V_G values ranging from 0 to 70 V demonstrate a linear behavior that indicates an ohmic contact. To generate charge-trapping states (in-gap traps) on the surface layer without fully oxidizing it, the InSe FET device was then subjected to an indirect oxygen-plasma treatment. To verify the underlying physical mechanism of their proposed device, an *operando* investigation of the trapping and detrapping process on the top layer was performed using a scanning photoelectron microscope (SPEM) that combines the chemical and electronic sensitivities of X-ray photoelectron spectra (XPS) with a spatial resolution ~150 nm. Moreover, SPEM has the ability to reflect the local electrical potential surrounding the probed atom. This approach allowed to explore the role of surface oxides in device behavior through observation of the changes in binding energy for the device under working conditions. The *operando* SPEM measurement setup of their devices at **TLS 09A1** beamline is illustrated in **Fig. 1(a)** (see next page). The device was scanned using a focused X-ray beam with spot size ~100 nm in ultrahigh vacuum conditions. To enable *operando* SPEM measurements during device operation, both source and drain electrodes were grounded; the gate electrode was subjected to a power bias.

To verify the van der Waals gating effect, they performed *operando* SPEM measurements at the oxygen plasma-treated channel. Upon application of a V_G 50 V, all signals moved to lower energies. To verify the trapped charge-induced core-level shifts, the In 4*d* and Se 3*d* binding energies are expressed relative to the In $4d_{5/2}$ and Se $3d_{5/2}$ signals, respectively. The relative energy difference between